PROCEEDINGS, 49th Workshop on Geothermal Reservoir Engineering
Stanford University, Stanford, California, February 12-14, 2024
SGP-TR-227

Evolution of a Geological Model for Co-Producing Electricity at the Blackburn Oil Field, Nevada

Abra Gold[1*], Estefanny Davalos-Elizondo[1], and Kagan Kutun[1]

[1]National Renewable Energy Laboratory, 15013 Denver West Parkway, Golden, CO, 80401, USA

Abra.gold@nrel.gov[*]

Keywords: Basin and Range province, Devonian reservoir, fault system, geological model, reservoir simulation

ABSTRACT

Oil fields characterized by significant proportions of hot water in the reservoir offer a unique opportunity for geothermal energy co-production and utilization. Development of an accurate geological model is essential in understanding the subsurface. However, this is a challenge at the preliminary stages of resource assessment when data on the subsurface parameters and subterranean fault network is scarce. Our focus in this paper is to explore a methodology for developing an accurate conceptual geological model representing the complexly faulted reservoir at the Blackburn Field, Nevada, to create a numerical simulation that will eventually be used to assess the potential of co-producing electricity. There are four steps to the evolution of this model: (1) collection of public data and research on the geological setting of the system; (2) digitization of seismic time-interpretation and cross sections to create the most representative model of the subsurface; and (3) creation of a natural-state numerical model to simulate the thermal gradient through the subsurface. Utilizing publicly available data of the geological system and the commercial Leapfrog Energy 3D subsurface geologic modeling software, we refined a preliminary geologic model to be more representative of the subsurface geology of an active geothermal exploration stage project. The conceptual geological model developed has been imported into VOLSUNG reservoir modeling software to create a natural-state model, further characterizing the Blackburn Field reservoir's thermal gradient. In the future, new seismic data will be utilized to further evolve the conceptual geological model for numerical simulations.

NOMENCLATURE

Table A: Nomenclature used throughout the publication.

English Symbols	Definition
A_{ij}	Surface area between elements i and j
c_p	Specific heat capacity
F^{κ}	Mass or heat flux
F_{ij}^{k}	Flux component
M^{κ}	Accumulation of mass or energy per unit volume
M_i^{k}	Accumulation of mass
n	Normal vector
P	Pressure
q	The source/sink contribution variable
Q_i^{k}	Component source or sink rate
T	Temperature
T_c	Temperature of reservoir cell
V_i	Volume of element i
V_n	Flow system sub-domain
X	Coordinate point in the X dimension

$X_{l,g}$	Mass fraction of liquid to gas
Y	Coordinate point in the Y dimension
Z	Coordinate point in the Z dimension
Greek Symbols	
Γ_n	Closed surface
κ	Mass component
λ	Thermal conductivity
ρ	Density

1. INTRODUCTION

Conceptual geological models (CGMs) have been utilized to characterize reservoirs for over 30 years. The effectiveness of this approach is exemplified by the work of Ayling and Hinz (2020), where they employ a conceptual model to characterize one of three geothermal resources in Hawthorne, Nevada, by gathering previous geological studies (including a previously developed 3D CGM) to estimate the geothermal potential of prospect A. With the emergence of new software and the growth of the geothermal industry, the use of 3D CGMs to characterize geothermal systems has become standard industry practice. An initial model is built to characterize the resource, which will be continually updated and evolved as more data becomes available. For instance, in a study conducted by Oviedo et al., (2023) thermohydraulic properties of rock units, petrographic analysis, and a 3D CGM of the Colombian Nevado del Ruiz geothermal system were added to the current CGM to improve overall understanding of the Nevado del Ruiz geothermal resources. When the CGM is improved as more data is added, such as subsurface data from first exploratory wells, higher resolution is attained, further improving the accuracy in evaluating the geothermal potential of a resource.

Challenges in the development of CGMs include inaccessibility of key subsurface datasets, lack of enough geological research conducted in an area, and lack of a proper data integration platform (Cavero et al., 2016). The resolution of some older cross sections, and the outdated representation of the data, may render the research incompatible with a 3D CGM. Additionally, privately owned data is difficult to obtain. As a result of data scarcity and uncertainty, most conceptual models are not entirely accurate and there is always opportunity for improvement and incorporation of new data.

The work site of this project is the Blackburn Field, Nevada, which has been producing oil since 1982. The oil field has a cumulative water cut of 90.91% over 30 years (1982–2022; Kutun et al. 2023). Recent field data suggests that the bottom hole temperature is approximately 260°F (127°C). On the site there are 20 wells, of which 17 are used to constrain the geological top boundaries (formation tops) of the different lithologies in the subsurface. The wells that are relevant to the development of the 3D CGM are Blackburn No. 1, 2, 3, 4, 5, 6, 10, 12, 14, 15, 16, 17, 18, 19, 20, 21, and Stream 1-7. Blackburn No. 1, 5, and 6 wells do not breach the hydrothermal reservoir. The only currently in-use wells are 3, 10, 12, 14, 16, 18, 19, 21, and 22; wells 12 and 21 are injectors, while the rest are either shut-in or producers (Kutun et al. 2023). Wells that breach the reservoir reach on average 7,525 ft (approx. 2,290 m) depth.

To demonstrate an improved workflow for geothermal resource assessment, we have developed a 3D CGM for Blackburn Field prior to the numerical modeling phase. In the workflow we integrate all data sets from various geothermal exploration stages into a geological model in Leapfrog, which is then introduced to VOLSUNG as the basis for the natural-state numerical reservoir model. In the first phase of our approach, we utilized publicly available data to develop an initial geological model. We evolved the model in the second phase by adding private data provided by Gradient Geothermal Inc. and created a seismic-based approximation of the subsurface using a time-evolved fault map of the Devonian reservoir. In the third phase, we created a natural-state reservoir model to simulate the thermal gradient through the subsurface. Our project shows that utilizing publicly and privately available data of the geological system and Leapfrog conceptual modeling software, it is possible to create a preliminary geological model of the subsurface and evolve the model into a more representative version over the course of an active geothermal exploration stage.

1.1 Basin and Range Geology and Tectonics

The Basin and Range province encompasses Mexico in its southern-most extent, portions of New Mexico, Arizona, California, Utah, Idaho, and nearly all of Nevada. In the Cretaceous period, the great Basin and Range province was likely a high orogenic plateau, leading to missing units in the geologic records of the region caused by erosion (Porter et al., 2014). The Great Basin experienced two distinct phases of volcanism: an ignimbrite flare-up beginning between 55-40 Ma which lasted until 18 Ma, and basaltic volcanism that began after 17 Ma associated with Basin and Range extension (Porter et al., 2014). Tectonically, this region evolved from a compressional zone to an extensional zone. There were two major extensional phases during the formation of the Basin and Range province: Eocene to Oligocene epoch relaxation of the crust caused by slab-rollback from approx. 55 to 20 Ma according to Bahadori & Holt (2019), and the 18 Ma subduction-to-extensional transformation of the Pacific-North American-Farallon plate boundary (Porter et al., 2014). The tension caused by the current plate boundary not only causes slip along the San Andreas Fault, but also contributes to the seismically induced faulting in the Walker Lane (Pedersen, 2023). As a result of these extensional stages, the Great Basin (which is a sub-region comprised mostly of Nevada) has exceptionally high heat flow caused by the thin nature of the crust (Porter et al., 2014). The central Great Basin

region, where Blackburn Field is located, contains a broad expanse of complex normal faulting (Faulds et al., 2006; 2013). The NNE-striking faults, as well as relay ramps or step-overs, are unique structural characteristics of Basin and Range extension (Faulds et al., 2006; 2013). Relay ramps and step-over zones are common in the Great Basin and can represent favorable structural settings for thermal water up-flow zones, as there are many (often quadrilateral) fault intersections along which fluids can travel through (Faulds et al., 2013). This region also experiences diffuse WNW-striking oblique-slip faulting from the Walker Lane fault belt (Faulds et al., 2006).

1.2 Geological History of Blackburn Field

The depositional subsurface units present in the Blackburn Field, from oldest to youngest units, are as follows: Nevada dolomite, Dale-Chainman shale, Indian Wells Formation, Humboldt Formation, Basalt Sill, and Hay Ranch Formation. A large-scale quartz monzonite pluton is also present. The Nevada dolomite is the reservoir of Blackburn Field. It is of upper-Devonian age and composed of hydrothermally altered dolomite that exhibits local brecciation, both macro and microscopic fractures, and micro to fine crystallization (Hulen et al., 1990). The Dale-Chainman shale is of Mississippian age and is composed of sandstones and organic shales unconformably overlying the Nevada dolomite (Hulen et al., 1990). Next in the stratigraphic sequence is the Indian Wells Formation, which is composed of poor to moderately welded tuff and tuffaceous sandstones deposited in the Oligocene, marking the first episode of volcanism recorded in the Blackburn Field (Scott & Chamberlain, 1988; Hulen et al., 1990). There is an approximate 300 Ma unconformity between the deposition of the Mississippian shales and Oligocene tuffs. The Humboldt Formation is composed of alluvial deposits, sandstones, and conglomerates, and chronologically follows the Indian Wells Formation in the stratigraphy (Hulen et al. 1990). A basaltic sill or spheroid body with unknown total extent, previously referred to by Hulen et al. (1990) as a dike, overlies the Humboldt formation, indicating a second later episode of volcanism in the Miocene epoch. Following this episode, the Hay Ranch formation is deposited, containing mud-rich lacustrine sediments, alluvial flows, and volcanics (Hulen et al., 1990; Flanigan, 1994). The quartz-monzonite pluton intersects Blackburn No. 1, 5, and 6 wells at bottom-hole depth and is a Cretaceous-age pluton emplacement that underlies part of the Devonian reservoir (**Figure 1**; Hulen et al., 1990; Flanigan 1994). The stratigraphic arrangement of these units is presented in **Figure 1**, and the thermal conductivity calculated for each unit based on previous studies is presented in **Table 1**. These thermophysical properties were used in the creation of the natural-state numerical model for analysis of the thermal gradient through the subsurface at Blackburn Field (see section 2.2.3).

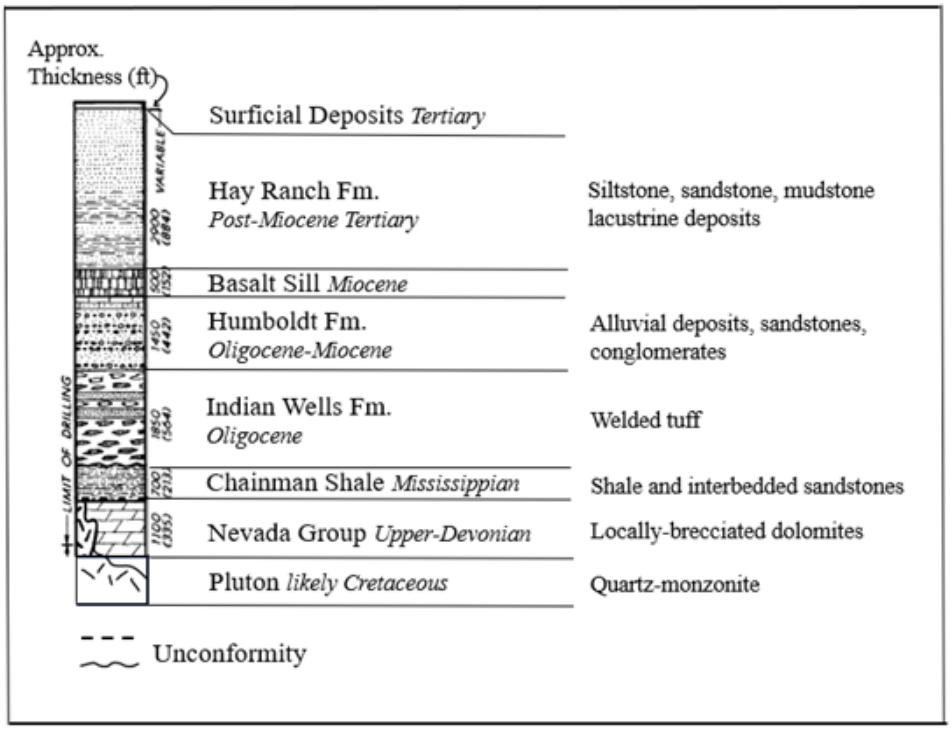

Figure 1: Stratigraphic column of the Blackburn Field geological units, adapted from Hulen et al. 1990.

Pre-Tertiary history of the area begins with the Devonian-Mississippian Antler Orogeny, a period during which the Devonian dolomites and other age-associated lithologies are thrusted on top of Mississippian source rocks (shales with sandstone lenses) in a complicated reverse-faulting and folding event (Hulen et al., 1990). Post-Antler Orogeny, the Mississippian Chainman shale unconformably overlies the Devonian dolomite reservoir and acts as a thin cap layer. An unconformity appears in the geologic record beyond this point in history, indicating up to a 300 Ma stage of limited deposition in the basin, extensive erosion, or both between the Mississippian and Late-Paleogene periods (Hulen et al., 1990; Flannigan, 1994). There was a wide-scale contractional folding event in the Miocene, which is evident in both the field and surrounding areas such as the Ruby Mountains East Humboldt Core Complex, located present-day within 100 miles north from the Blackburn Field (Snoke et al., 1997).

Table 1: Thermophysical properties of CGM units. If a range of thermophysical property values was provided in the source, the average of that range was calculated and is displayed in the table. If no range was provided, no average was taken.

Rock Unit	λ	c_p	ρ	Source	Source	Source
	W m^{-1} K^{-1}	kJ kg^{-1} K^{-1}	kg m^{-3}			
Granite	3.24	0.96	2630	Schön, 2011	Schön, 2011	Schön, 2015
Quartz Monzonite	2.76	0.879	2640	Davis et al., 2007	Waples, 2004	Waples, 2004
	3.05	-	-	University of Nevada, Reno, 2021	-	-
Basalte (Basalt)	1.82	0.88	2800	Schön, 2011	Schön, 2011	Schön, 2015
Dolomite	4.9	1	2710	Sass' et al., 1988	Schön, 2011	Manger, 1963
	4.15	0.9	2625	Schön, 2011	Waples, 2004	Schön, 2015
	4.9	-	2800	University of Nevada, Reno, 2021	-	Waples, 2004
Chainman Shale	2.07	1.18	2585	Schön, 2011	Schön, 2011	Manger 1963
	1.5	-	-	University of Nevada, Reno, 2021	-	-
Sandstone	2.92	1.64	2400	Schön, 2011	Schön, 2011	Schön, 2015
	-	0.775	2640	-	Waples, 2004	Waples, 2004
Limestone	2.9	1.64	2500	Schön, 2011	Schön, 2011	Schön, 2015
	3.26	0.68	2770	University of Nevada, Reno, 2021	Waples, 2004	Waples, 2004
	-	0.88	2760	-	Waples, 2004	Waples, 2004
Conglomerate	1.85	0.87	2520	Zhu et al., 2022	Zhu et al. 2022	Manger, 1963
	2.24	1.03	-	Zhu et al., 2022	Zhu et al. 2022	-
	1.32	-	-	University of Nevada, Reno, 2021	-	-
Playa Sediments	1.63	-	-	University of Nevada, Reno, 2021	-	-
Clay-Rich Units	1.025	-	-	Blackwell & Steele, 1989	-	-
	1.29	-	-	University of Nevada, Reno, 2021	-	-
Siltstone	2.675	0.91	2680	Schön, 2011	Waples, 2004	Waples, 2004
	1.42	-	-	University of Nevada, Reno, 2021	-	-
Sand	2.675	0.91	2680	Schön, 2011	Waples, 2004	Waples, 2004
	1.42	-	-	University of Nevada, Reno, 2021	-	-
Bedded Tuff (dry)	0.78	-	-	Sass' et al., 1988	-	-
	1.17	-	-	University of Nevada, Reno, 2021	-	-
Tuff	1.67	0.795	1850	Sass' et al., 1988	Waples, 2004	Schön, 2015
	1.9	1.09	2375	Blackwell & Steele, 1989	Waples, 2004	Schön, 2015
	1.82	-	2690	University of Nevada, Reno, 2021	-	Waples, 2004
	-	-	2750	-	-	Waples, 2004
Valley Fill	1.4	-	-	University of Nevada, Reno, 2021	-	-
	1.5	-	-	University of Nevada, Reno, 2021	-	-
	1.7	-	-	University of Nevada, Reno, 2021	-	-

1.2.1 The Devonian Reservoir

The Devonian dolomite at Blackburn Field exhibits extensive hydrothermal alteration episodes. Hydrothermal alteration type and style are significant influences on thermal fluid flow, thermal history, and heat source. These are important datasets in developing a conceptual model for the Blackburn Field hydrothermal system. As reported by Hulen et al., (1990) it is evident that there were at least four brecciation episodes that were likely pre-historic. These episodes were followed by secondary mineralization of dolomite, locally occurring barite, quartz-pyrite, kaolin, and late-stage dickite (in depositional order from oldest to latest). The dolomite veins are localized as inferred by their absence in the Blackburn No. 10 well, where the oldest inclusions are quartz-pyrite-galena-sphalerite. Fluid inclusions in dolomite and barite hosted veinlets indicate a homogenization temperature of 662 to 764°F (350 to 407°C). These high temperatures likely suggest primary inclusions associated with vein emplacement. The other population of early vein dolomite and barite fluid inclusions indicate a homogenization temperature of 228 to 268°F (109 to 131°C; Hulen et al., 1990), which is more akin to a hydrothermal system. It is worth mentioning that the conditions for oil generation in the subsurface were not reached until 8 Ma, and the temperature of oil did not reach 220°F (104.44°C) until 1.5 Ma (Flanigan, 1994).

A plutonic quartz monzonite body is evident in both the history of Blackburn Field and in the well logs (Scott & Chamberlain, 1988; Hulen et al., 1990; Flannigan, 1994; NBMG 2023). The Devonian reservoir rock unconformably overlies the quartz monzonite body. Flanigan (1994) also states that the Quartz-Monzonite pluton was Pb-K dated back to the Cretaceous period, as reported in a previous release of unpublished data. Hulen et al. (1990) notes that Jurassic-Cretaceous plutonic bodies had been associated with hydrothermal alteration in previous studies, and were found to have had high-temperature, high-salinity two-phase alteration in dolomitized segments of the Upper Nevada formation. Despite this, it is not probable that the driving force of thermal recharge in this system is from the pluton, as the pluton intruded in the late Cretaceous, and while it may have altered the dolomite, would not have the thermal potential required to produce the temperatures (260°F, 125°C) that are seen at depth today (Hulen et al., 1990). Hulen et al. suggested that the geothermal fluid is deep convection-driven, and that the fluid may be upwelling along the Sulphur Springs Range westernmost front, where normal faults are abundant (1990).

1.3 Structural Geology of the Blackburn Field

The Blackburn Field is considered a part of the central Basin and Range province and was affected by at least two outlying regions: diffuse NW-striking right-lateral faults and north-striking normal faults from Walker Lane, as well as NNE-striking normal faults and ENE-striking oblique-slip faults. The shear stress from Walker Lane has been reported to dissipate through the province, which may explain the fault planes seen at depth and in surface traces of faults present at the Blackburn Field (Flanigan, 1994; Faulds et al., 2006). Additionally, the Blackburn Field is located within the Humboldt Structural Zone, which contains ENE-striking oblique-slip fault orientations; in early publications, similarly striking faults are indicated at the Blackburn Field (Scott & Chamberlain, 1988; Hulen et al., 1990; Flannigan, 1994; Faulds et al., 2006). The most established fault in the field is the Blackburn fault, an N-S striking normal fault that, according to publicly available data, terminates slightly to the southwest of the Blackburn Field well cluster 3 through 21, excluding wells 5 and 6 (**Figure 2**). Another fault extends sub-parallel to the Blackburn fault and is N-S striking, creating a zone of complex faulting with documented fracturing (Hulen et al., 1990). Two faults trending in the same manner, terminating within the same block of space, interrupted by feathering of fault structures between them, is indicative of a relay ramp or step-over zone (**Figure 2**; Faulds et al., 2013). At least one E-striking fault bounding the northern sector of the reservoir rock and another NW-striking fault to the south of the well cluster intersects the Blackburn fault and reportedly terminate against the Blackburn fault (Scott & Chamberlain, 1988; Flanigan, 1994).

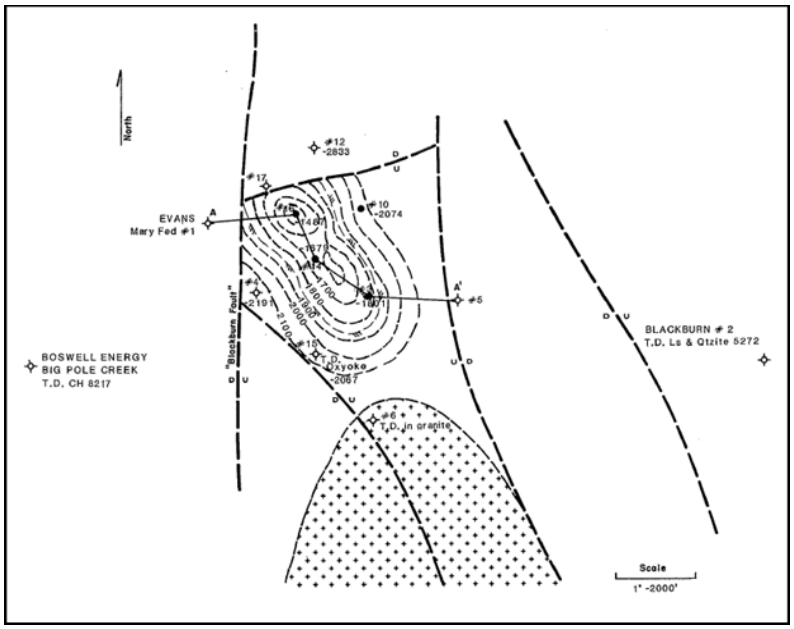

Figure 2: Preliminary map of the quartz monzonite pluton structure adapted from Scott & Chamberlain 1988.

In 1990, Hulen et. al. proposed a conjectural view of the subsurface in two cross sections. While these cross sections were based partially on an interpretation from Scott & Chamberlain (1988), they are not a reflection of seismic data (**Figure 3B**). Flanigan (with operator modifications) offered a time-elevated fault map of the subsurface that was provided as an unpublished release of data from Grant Canyon Oil and Gas LLC, and is an interpretation 3D seismic (**Figure 3A**). This map suggests a few changes in dipping of faults from Hulen et al. (1990) and identifies more trends of fault scarps than the cross sections proposed in 1990. In the time-elevated fault map, 11 faults are represented in the system and are downthrown to the west. All faults trending NNE-SSW dip toward the West, which is expected in a step-over zone. The faults trending NNW-SSE dip toward the North, excluding the fault affectionately named major Blackburn Terminator fault (terminates against the major Blackburn Fault in the southeast; **Figure 2**) which is indicated dipping to the south in the time-elevated fault map and the cross sections (**Figure 3**; Hulen et al., 1990; Flanigan, 1994). The faults are primarily high-angle normal faults (dipping at an angle of 70° to 80°, most likely) as recorded in Scott & Chamberlain (1988) and Hulen et al. (1990). The fault system in the time-elevated map intersects frequently and provides abundant pathways of thermal fluid upwelling.

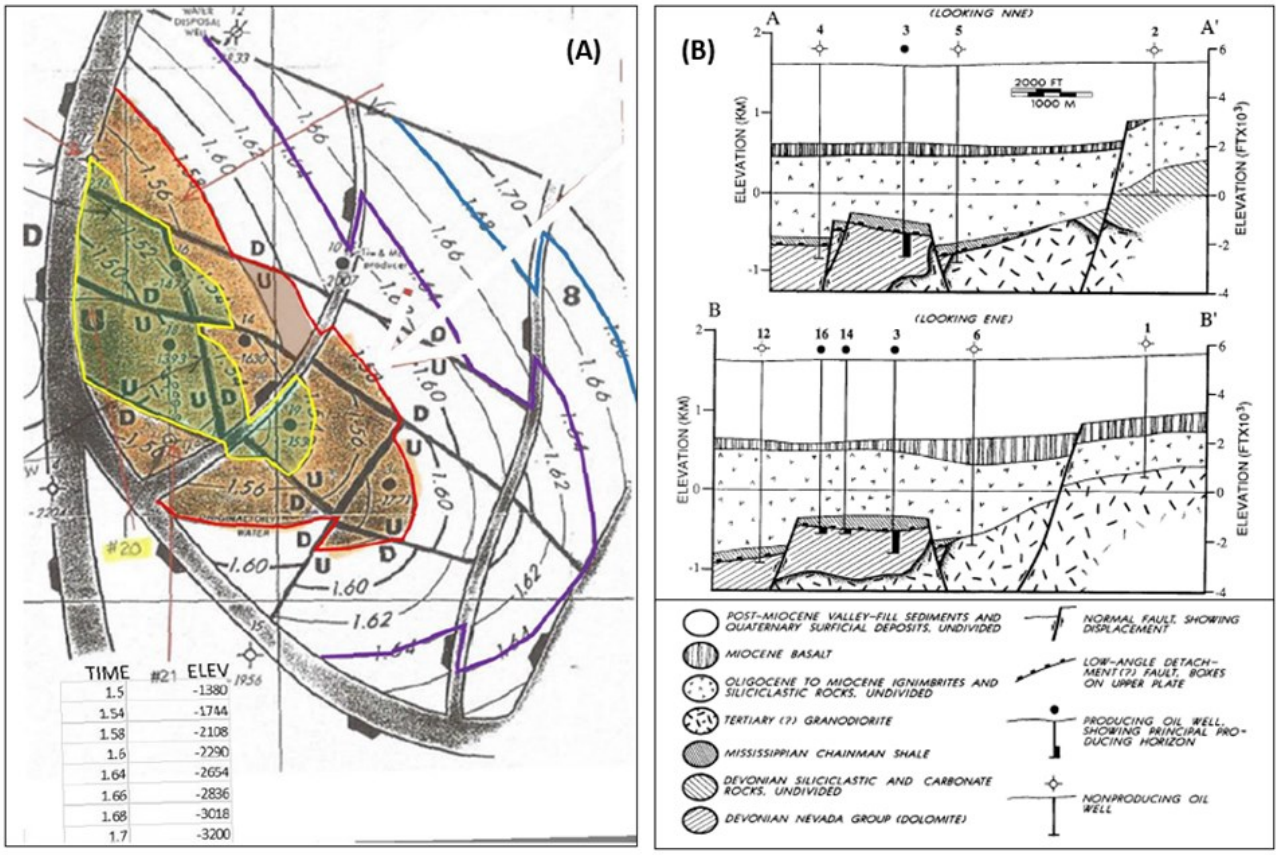

Figure 3: (A) Fault blocks of the dolomite reservoir developed by Flanigan (with modifications by operator) based on 3D seismic data (unpublished). (B) Cross-sectional interpretation of the subsurface, adapted from Hulen et al. (1990).

According to Flanigan (1994), fault interceptions occur at Evans No. 1 Mary Kay well, and Blackburn No. 2, 3, 4, 6, 15, 16, 17, and 18 wells. In total, six faults intercept these wells (**Table 2**). The fault intersections at Evans No. 1 Mary Kay well (which is assumed to have been re-named Mary Kay - Federal Unit 1 in current day records) and Blackburn No. 2 well were excluded from the table, as they fell outside of our modeling region. Therefore, Faults A and F are also not modeled, as they only intersect wells outside of the study. The fault-well intersections reported by Flanigan (1994) were used to check generally where faults and wells should intersect; exact matches to the measured locations of fault-well intersections were not included, as determining which faults were related to "Fault B, C, D, or E" induced uncertainty; there were beyond four faults represented in the structural fault map, and the faults in this model extended through the capping layer only.

Table 2: Fault intersections based on downhole well logs, adapted from Flanigan (1994).

Well-Fault Intersections	No. 3	No. 4	No. 6	No. 15	No. 16	No. 17	No. 18
	ft (depth)						
Fault B	-	6690	-	-	3790	7245	3755
Fault C	5410	-	-	7280	-	-	-
Fault D	7553	-	-	-	-	-	-
Fault E	-	-	3810	-	-	-	-

2. METHODS

2.1 Conceptual Geological Model

2.1.1 Phase 1: Public Data Interpretation

At the start of the project, limited data was available: the use of public well cuttings logs, downhole seismic logs, resistivity logs, geological studies from the '80s and '90s, and a map of the surface topography of the Blackburn Field was crucial in creating the CGM. The reported tops of geological formations were re-evaluated and confirmed with the available resistivity, mud, and cuttings logs, and then developed into a lithology survey to be imported into the Leapfrog 3D CGM. Blackburn No. 1 was utilized briefly in the earliest conceptual model to project the trend of the quartz monzonite pluton, as few wells encountered the pluton. One possible surface-expression of the field was also identified: a gas seep located near the base of the neighboring Sulfur Springs Range (**Figure 4**; Hulen et al., 1990; Flanigan, 1994). Using the lithology survey, the well lithologies were imported and a preliminary model of the subsurface stratigraphy was generated.

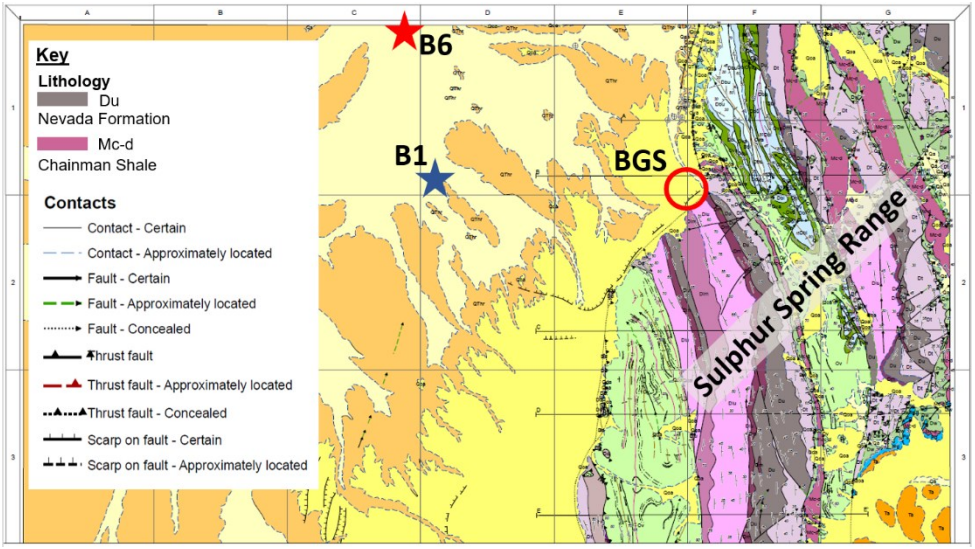

Figure 4: Regional Geologic Map displaying the location of the Bruffey Gas Seep (BGS), the wells Blackburn 1 (B1) & Blackburn 6 (B6). Adapted from Kutun et al. (2023) and Carlisle & Nelson (1990).

The two cross sections from Hulen et al. (1990) as well as the top of the quartz monzonite body from Scott & Chamberlain (1988) were both utilized in importing the first four faults into the model: the prolific Blackburn Fault, which appears on all cross sections, the Blackburn Terminator Fault, Fim Fault, and Fault Seventeen (**Figure 5**). These names refer to the four original faults mapped in the first phase of the project; future faults were too numerous to name and have been assigned the typical "F-1" notation (e.g., Fault 1). The cross sections, being from different publications, were not aligned with each other. To import them into the model, the wells indicated in both the cross sections and the quartz-monzonite top map were aligned with the Leapfrog well data to create the best-fit approximation of each data type. There was a discrepancy between the two public-study cross sections, and because neither of the cross sections were based entirely on seismic, an approximate distance between the two figures was allocated for Fault Seventeen. The Blackburn Terminator Fault is shown dipping SW, as the second cross section from Hulen et al. (1990) looking NNE indicates. The Blackburn Terminator Fault is placed along the trend proposed by Scott & Chamberlain (1988) with a dip angle that approximately matches the angle shown in the NNE cross section (Hulen et al., 1990). The most significant fault for hydrothermal fluid upwelling is the Blackburn Fault, and the most likely intersection for upwelling is that of the Blackburn Terminator with the Blackburn Fault because both faults are shown as dilated on Flanigan's time-elevated fault map (with modifications by operator).

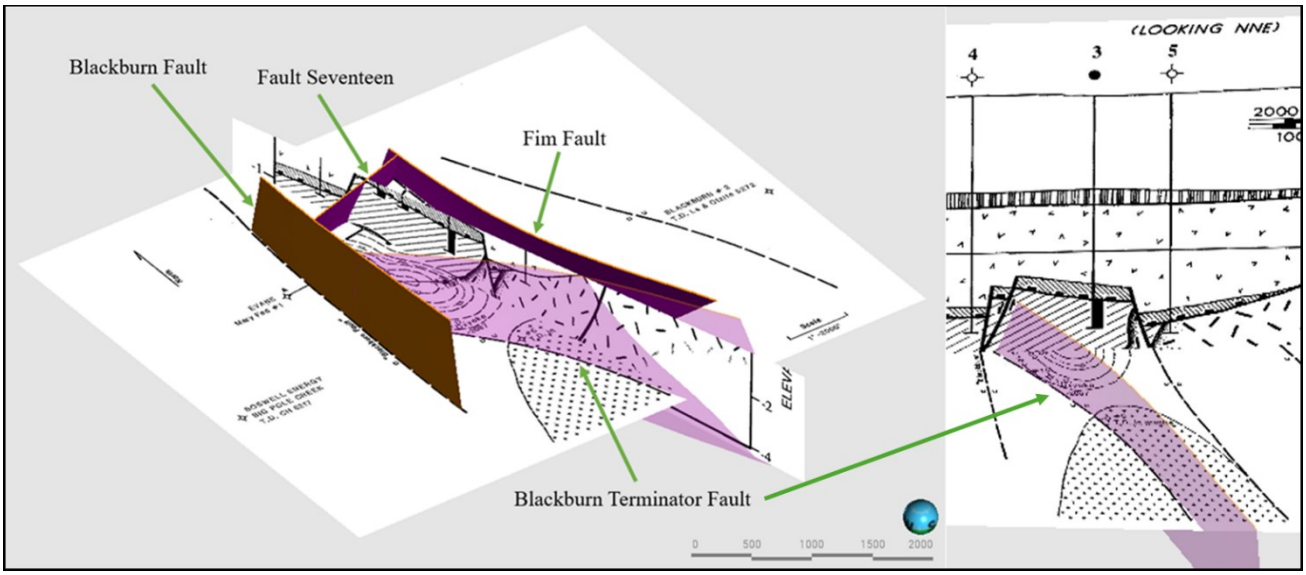

Figure 5: Propagation of faults based on imported cross sections (Hulen et al., 1990) and a map of the quartz monzonite pluton (Scott & Chamberlain, 1988) looking ENE and NNE. The Blackburn Fault terminates before the end of the map because the model extents did not include that portion of the subsurface, as the reservoir rock terminates against the quartz monzonite.

2.1.2 Phase 2: Private Data Interpretation

To complete this phase, the time-elevated fault map developed by Flanigan (with operator modifications) was utilized (**Figure 3B**). Importing the interpretation of the subsurface at the depths corresponding to the isotherms in the time-elevated map did not result in downhole well alignment from the drill logs. To avoid distorting the imported map in Leapfrog and increasing uncertainty in fault locations, the best-fit approximation of the fault map was utilized by aligning the central cluster of wells in the map to the bottom hole locations reported in drill logs. The fault blocks were structured to follow the fault lines on the time-elevated structural map of the Devonian reservoir. After structuring and aligning these faults, the block surfaces were edited with polylines to constrain the tops of both the Chainman capping layer and the Devonian reservoir to the tops of the formations reported by the drill logs. To determine the confidence with which to regard the time-elevated structural interpretation, an analysis of the surface DEM from USGS (2018) was searched for fault scarps at the surface that could match faults reported in the Devonian reservoir (**Figure 6**).

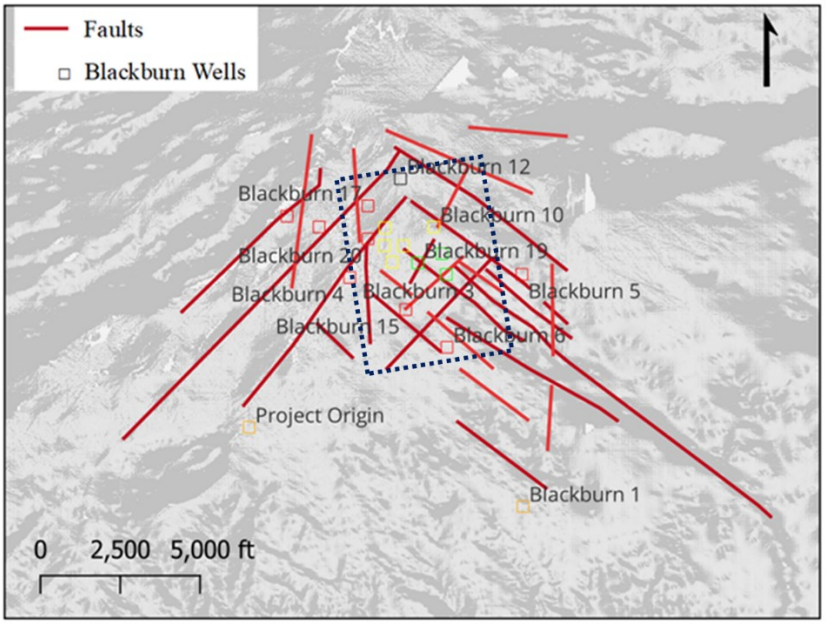

Figure 6: Propagation of fault scarps as interpreted from DEM data (10 m), adapted from USGS (2018). Note propagation of ENE-, N-, and WNW-striking faults related to Basin and Range tectonics. The dotted rectangle is the extent of the time-elevated fault map, and the focus of both the CGM and numerical simulation.

Additionally, the Leapfrog geological and VOLSUNG numerical model extents were modified to better fit the well data available from drill logs, so that the bugs in the numerical model would be reduced while producing and injecting wells close to the boundary of the CGM volumes. The CGM was extended to the north and reduced in the south, giving wells ample room to produce or inject, and cutting out inactive space in the numerical simulation to improve the computation time of simulation states. The faults were constrained to the top of the capping layer, and the overlying layers remained conductive for the purposes of this project. Conductive overlying layers with sealing faults most likely exist, as the valley-fill sedimentary layer would allow for the filling-in of more recent faulting with overburden.

2.2 VOLSUNG Brynhild Natural-State Model

2.2.1 Mass-Energy Conservation & Physical Phenomena Simulated

Mass and energy were conserved by the balances of the Fafnir reservoir simulator utilized in VOLSUNG (Volsung User Manual, 2023), which operates on the conservation equations shown by Pruess et al. (1999), expressed by:

$$\frac{d}{dt}\int_{V_n} M^\kappa dV_n = \int_{\Gamma_n} F^\kappa \cdot n d\Gamma_n + \int_q q^\kappa \cdot dV_n \tag{1}$$

where V_n is the sub-domain of the flow system, Γ_n is a closed surface, M^κ is accumulation of mass or energy per unit volume, κ=1, …, NK mass components (for a single-phase fluid, κ=1) and κ=NK +1 heat components, F^κ is mass or heat flux, q is the source/sink contribution, and "n" is a normal vector on Γ_n that points inward to V_n. The conservation of mass and energy in Fafnir includes the balancing of source and sinks attached to the computational element or neighboring elements (Equation 4.6 Volsung User Manual, 2023):

$$\frac{dM_i^k}{dt} = V_i^{-1} \cdot \left(\sum_j A_{ij} F_{ij}^k + Q_i^k \right) \tag{2}$$

where M_i^k is the mass accumulation of (in the case of this model) water, V_i^{-1} is the volume of element i, A_{ij} is the surface area between elements i and j, F_{ij}^k is the flux component between elements, Q_i^k is the component source or sink rate.

The physical flow phenomena simulated was single-phase pure water, where the fluid pressure and temperature were within the thermodynamic range of the table utilized by the simulator. This assumption of pure water is an approximation, as reported fluid salinity did not exceed 5% according to a well completion record obtained from NBMG (2023), and the pressure is high enough to constrain the fluid to a single phase both at depth and as it ascends through the wellbore. Accumulation of fluid mass in available pore space functions by the conservational equations described by Pruess et al. (1999). To simulate a dual-porosity model, the MINC (multiple interacting continua) approach was utilized, which governs fluid transport through pores and fractures under the assumption that fluid travels faster through permeable fractures than through porous matrix blocks, therefore changes in reservoir conditions are determined by flow through fractures and fracture-matrix block local interactions (Pruess, 1992).

The physical heat transfer phenomena simulated were conduction in the "fill" layers (Indian Wells, Humboldt, Basalt, Hay Ranch/Valley Fill), and convection in the reservoir. The lack of convection in the upper fill layers of the model was supported by the sealed faults that may exist in the upper units of the field caused by sedimentary overburden infilling. Like the accumulation of fluid mass, accumulation of heat stored in both the rock and fluid also operates on conservation equations shown by Pruess et al. (1999). The MINC approach allows heat transport and pressure support through matrix blocks to fractures (Volsung User Manual, 2023).

2.2.2 Model Geometry

The spatial extents of the TARTAN reservoir grid are determined by the extents of the Leapfrog model (**Table 3**). After testing multiple grid sizes, we determined that the grid size selected is representative of a model that produces accurate results in an optimal timeframe. The vertical thickness of each individual grid square is 60.9 m.

Table 3: TARTAN grid constraints.

Grid Extents	*X* m	*Y* m	*Z* m	*X* ft	*Y* ft	*Z* ft
Minimum Corner	570,988	4,451,450	-1,310.64	1,873,320	14,604,500	-4,300
Maximum Corner	574,200	4,455,630	1,613.92	1,883,858	14,618,210	5,295
Δ (*X, Y, Z)*	3,212	4,180	2,924.56	10,538	13,710	9,595

2.2.3 Material Properties

Material properties for geological units were derived from publicly available data (**Table 4**). Where data points for thermophysical properties taken in Nevada were available, these datapoints were utilized in the geological properties of the natural-state simulation. If no local Nevada data points were available, averages of generalized data for the rock type of the formation were utilized. To estimate the thermophysical properties of the Humboldt and Fill (Hay Ranch) formations, which included multiple rock types, two downhole cuttings logs were utilized to determine the thickness of each independent lithology inside of the formation. A thickness-weighted average of the thermophysical properties was calculated for both formations based on the cuttings. Each property was mapped to an element within its associated conceptual geological model volume.

Table 4: Thermophysical properties of geological units for the assignment of thermophysical properties.

Geological Unit	λ	c_p	ρ
	W m^{-1} K^{-1}	kJ kg^{-1} K^{-1}	kg m^{-3}
Quartz Monzonite	3.05	0.879	2640
Nevada Dolomite	4.90	0.950	2712
Chainman Shale	1.50	1.180	2585
Indian Wells	1.74	0.943	2416
Humboldt	1.82	1.109	2525
Basalt	1.82	0.880	2800
Fill (Hay Ranch)	1.72	1.089	2547

Faults were imported as geological barriers, or 2D polygons that controlled secondary permeability through faults and fractures. These barriers, or faults, were simulated as permeable in the natural-state model. In Leapfrog, when faults terminate against another fault, the fault is clipped. Therefore, in the numerical model the faults reported in Flanigan's time-evolved structural map (with operator modifications) are reflected in segments, as many of the faults have terminated against neighboring faults and were displaced; the segments were imported as individual fault meshes. The faults in the natural-state simulation are considered sealing, or non-permeable, faults. The permeability of the reservoir and the pluton in the z-dimension has been increased to simulate densely fractured geologic units, as this is the likely case of both units in the Blackburn Field.

2.2.4 Reservoir Boundary Conditions

Boundary conditions selected for the natural-state model were a constant pressure and fluid flow condition to simulate a steady-state reservoir. A bottom constant pressure condition was simulated to replicate a steady-state reservoir. The bottom constant pressure and bottom hot plate boundary conditions were assigned to the base of the reservoir, while an atmospheric boundary condition constrained an ambient surface temperature and pressure to the top of the model. The bottom constant pressure boundary condition was selected based on a static reservoir pressure estimation from a well flowing test.

Table 5: Boundary conditions for the natural-state simulation.

Boundary Condition	P	T	P	T
	psi	°F	Pa	°C
Bottom Constant Pressure	4175	276.3	2.88e+07	136
Bottom Hot Plate	-	276.3	-	136
Atmospheric Boundary	14.7	54.7	1.01e+05	12.6

2.2.5 Natural-State Simulation Scenario

The natural-state simulation scenario was a sealing-fault model that simulates a thermal gradient through the subsurface with the assumption that faults are non-permeable. Permeability in the z-dimension has been set to simulate a densely fractured reservoir and pluton. Sealing faults may not be the case in the actual reservoir, as some, or all, of the fault blocks may be connected and large fault dilations are present in the time-elevated fault map (Flanigan, with operator modifications).

3. RESULTS

The geological model of the Blackburn Field was developed based on the geological and structural history of the local site and region, as well as formation tops determined from well logs by Taverna (2019) that were cross-checked and reconfirmed before defining the formations. The quartz-monzonite pluton partially underlies the Nevada dolomite reservoir, which are both heavily faulted bodies of rock. The Nevada dolomite faults follow the orientations proposed by Flanigan (with operator modifications). The quartz monzonite faults follow the orientations from the cross sections developed by Scott & Chamberlain (1988) and Hulen et al. (1990), as a large portion of the pluton is outside of the time-elevated fault map's boundaries. Overlying the dolomite is the Chainman shale, which is considered the capping layer, and follows the fault orientations proposed by Flanigan (with operator modifications). The faults have not been extended beyond the reservoir and capping layer for multiple reasons: (1) the reservoir is the main focus for our numerical modeling purposes; (2) there is an unconformity between the Chainman Shale and Indian Wells formations, and it is not possible to tell which modeled faults occurred during the unconformable period or after the period; and (3) the extent of each modeled fault into the overlying formations is not able to be interpreted from available cross sections. Therefore, after the Chainman Shale, the overlying lithologies are the Indian Wells, Humboldt, Basalt Sill, and Hay Ranch formations.

It is apparent that the source of the heat flow in the Blackburn Field is not pluton-driven and is instead deep-convection driven (Hulen et al., 1990). There is already evidence of multiple episodes of hydrothermal alteration, which the plutonic intrusion may have contributed to, but historically the field has been controlled by a deeper geothermal heat source likely driven by the regional tectonics and thinner crust. Thick overlying sediment traps could also provide conductive insulation for the fluids in the reservoir and control the transport of heat through the subsurface. Faulds et al. (2006) suggest that fields in Nevada are controlled by diffuse WNW-directed extension from the Walker Lane fault belt, and Northern Great Basin WNW extension, allowing for high fracture densities and dilation of NNE-striking faults, allowing deep circulation of thermal fluids. High fracture densities in fields with multiple fault intersections in the subsurface (like the Blackburn Field) facilitate convection of fluids from a deep-seated heat source to the reservoir (Faulds et al., 2013). Therefore, it is also the case that the fluid does not necessarily have to be upwelling along the western front of the neighboring Sulfur Springs Range, but instead could be circulating directly beneath the field itself.

3.1 Conceptual Geological Model

3.1.1 First-Phase Public Data Model

The first model was created from publicly available data. This model follows the interpretation of the subsurface from one map of the quartz-monzonite pluton, and two cross sections of the Devonian reservoir (**Figure 7**). This first-stage, preliminary conceptual model captured the main faults presented by the reference cross sections and quartz-monzonite pluton map. The trend of the pluton in this model was interpreted from two down-hole formation tops of the quartz monzonite in Wells 1 and 6. In this model, the focus was to constrain the surface of the reservoir to the formation tops reported in the well logs, so the contact of the Nevada dolomite to the Chainman shale is slightly out of line compared to the cross sections. However, because the cross sections are interpretations and the formation top reports are based directly on mud-logs, the formation tops were honored in this model. Leapfrog superimposed the subsurface expression by interpreting the well log data, and the faults in the model. In areas where less data is present, the contacts may not be representative of the subsurface.

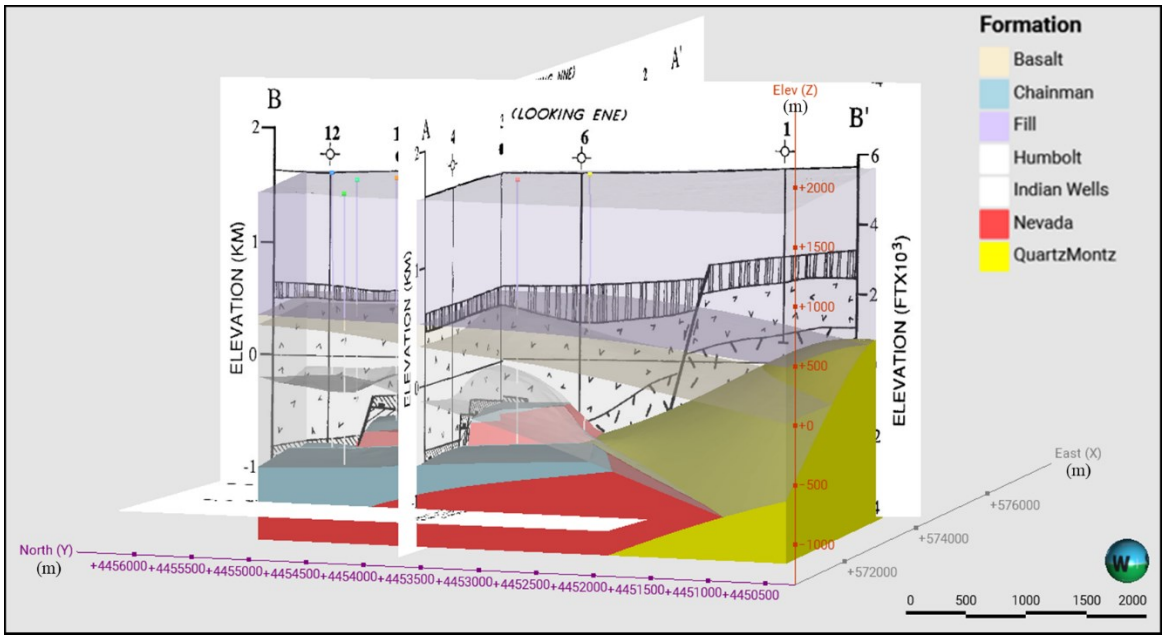

Figure 7: Initial, public-data generated Leapfrog 3D CGM for the subsurface at Blackburn Field, Nevada. In areas where no well data was available, contacts were inferred using Leapfrog's initial extrapolation of formation top trends and may not be representative of the subsurface.

3.1.2 Second-Phase Private Data Model

The second-phase CGM was created from privately available data. This geological model follows the interpretation of the subsurface from Flannigan's (1994) time-elevated structural map (**Figures 8, 9**). The well furthest toward the northwest (Blackburn No. 1) is now outside of the model boundaries, to constrain the model focus on the wells that breach the reservoir. The quartz-monzonite pluton is faulted according to the cross sections proposed by Hulen et al. (1990). All extrapolated contacts created by Leapfrog (in all fault blocks) were edited with polylines to better constrain the model formation tops to the formation tops reported in the well log files. External contacts, where no well clusters were present, were edited with polylines to create an interpretation that may be more representative of the subsurface than the contacts proposed in the previous first-phase, publicly sourced model. Interpretations in areas where no downhole well data is present may not be representative of the subsurface. This is because interpretation is not based on the tops of formations displayed by and picked from the downhole well logs. The tops of geological formations reported in the downhole well data are the only physical data points constraining the geological formations in the model, and are the most accurate state of knowledge of the subsurface. Therefore, in areas where no downhole well data is present, the interpretation is far less accurate. A depth interpretation of seismic cross sections provided by Grant Canyon Oil and Gas LLC was utilized to confirm that the minor faults bridging the step-over zone, between Fim Fault and the Blackburn Fault, were likely high-angle normal faults. These cross sections were in image format and were not geo-referenceable or physically imported into the model, as importing the section caused significant distortions. The cross section did however confirm that the minor ENE-trending bridge faults likely dipped to the north, or north-northeast.

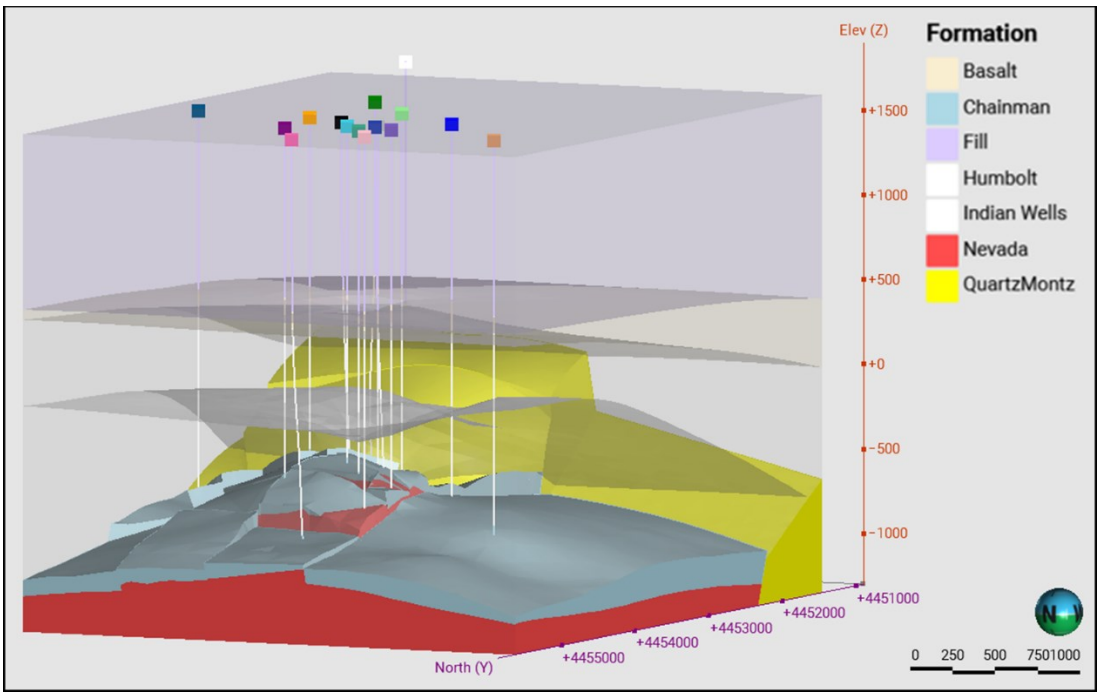

Figure 8: Second-phase, private-data generated Leapfrog 3D CGM for the subsurface at Blackburn Field, Nevada looking southeast. In areas where no well data was available, contacts were inferred using polyline editing of formation top trends and may not be representative of the subsurface. The colored blocks at the surface are wellheads. The colors match the same-colored blocks in Figure 9.

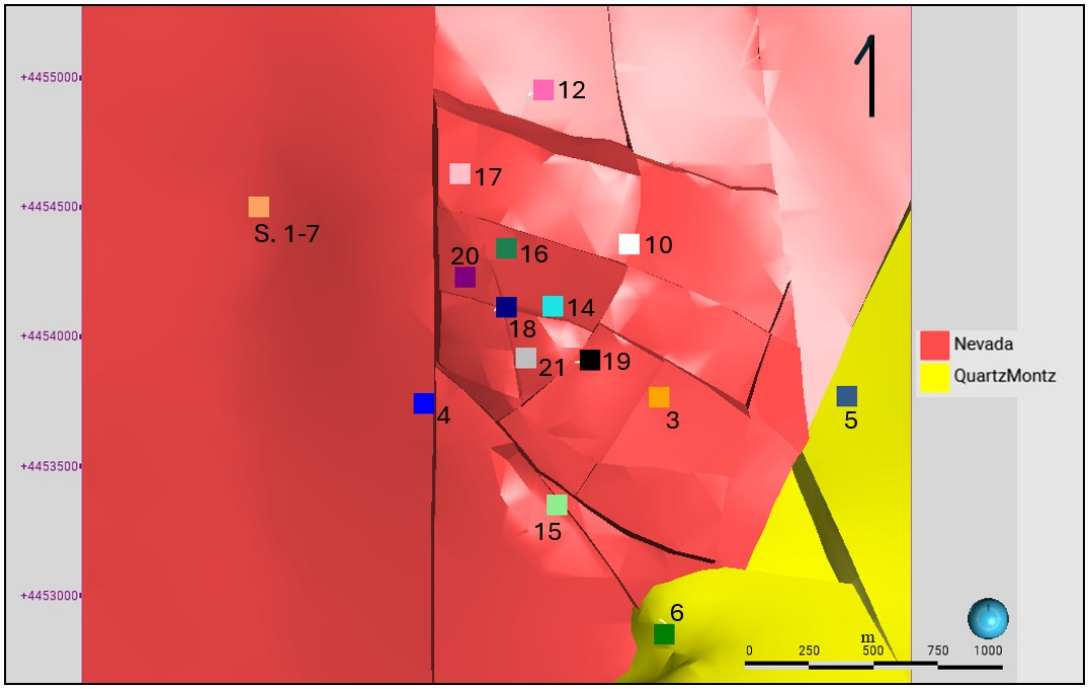

Figure 9: View of the fault blocks following the interpretation of Flanigan's time-evolved fault map (with operator modifications). Contacts were adjusted to follow formation tops reported in mud logs from the well log files. Numbers refer to respective wells.

The fault traces on the surface of the Blackburn Field display a likelihood of quadrilateral fault intersections at depth, as there are visible intersections of NE- and NW- trending faults. The traces also provide a degree of confidence in faults that are notated in the subsurface, however fault orientations can change at depth, and some faults in the subsurface may not extend entirely to the surface if they formed before the overburden was deposited. Recently obtained 3D seismic data will be utilized in the next phase to update the subsurface to a more-representative model, and to confirm the existence and location of faults from Flanigan's time-elevated interpretation of the subsurface (with operator modifications).

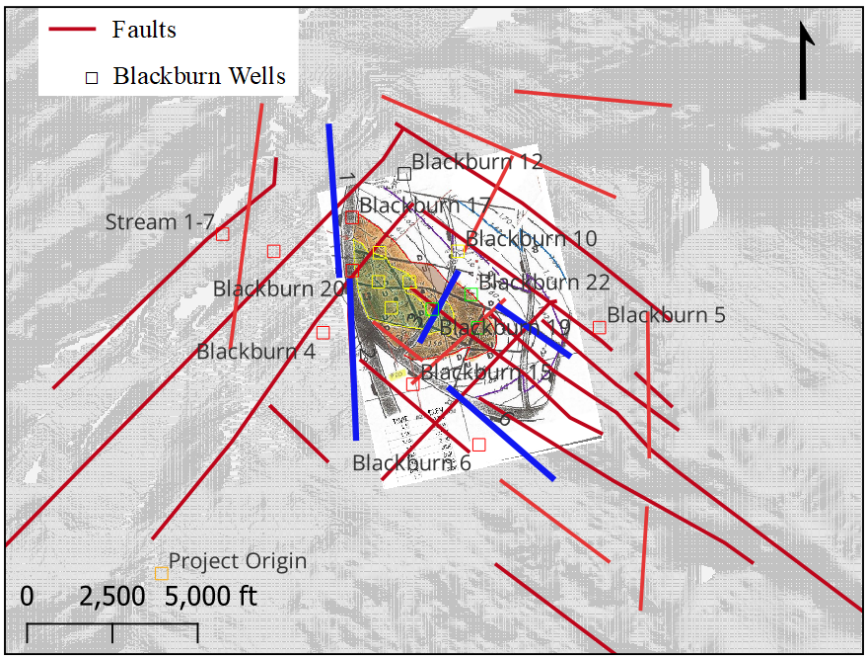

Figure 10: Fault scarp and subsurface confidence interpretation. Faults outlined in the thicker, darker blue color are faults that are more likely to exist in the subsurface, which also are represented by Flanigan's (with moderator modifications) time-elevated fault map.

3.2 Natural-State Numerical Model

The results of the natural-state numerical simulation are presented in **Figure 11**. The temperature at approximately 9,580 ft (2,920 m) depth is simulated as 298°F (147.8°C), while the temperature at the surface is 54.8°F (12.5°C). Convection in the reservoir and pluton disturbs this gradient, which is related to the simulated vertical fracture permeability, as shown by the inconsistent isotherms in **Figure 11**. The temperature of the Blackburn No. 18 wellbore-coupled cell, T_c, is 261.884°F, giving an approximate match of 262°F to temperatures observed in the field.

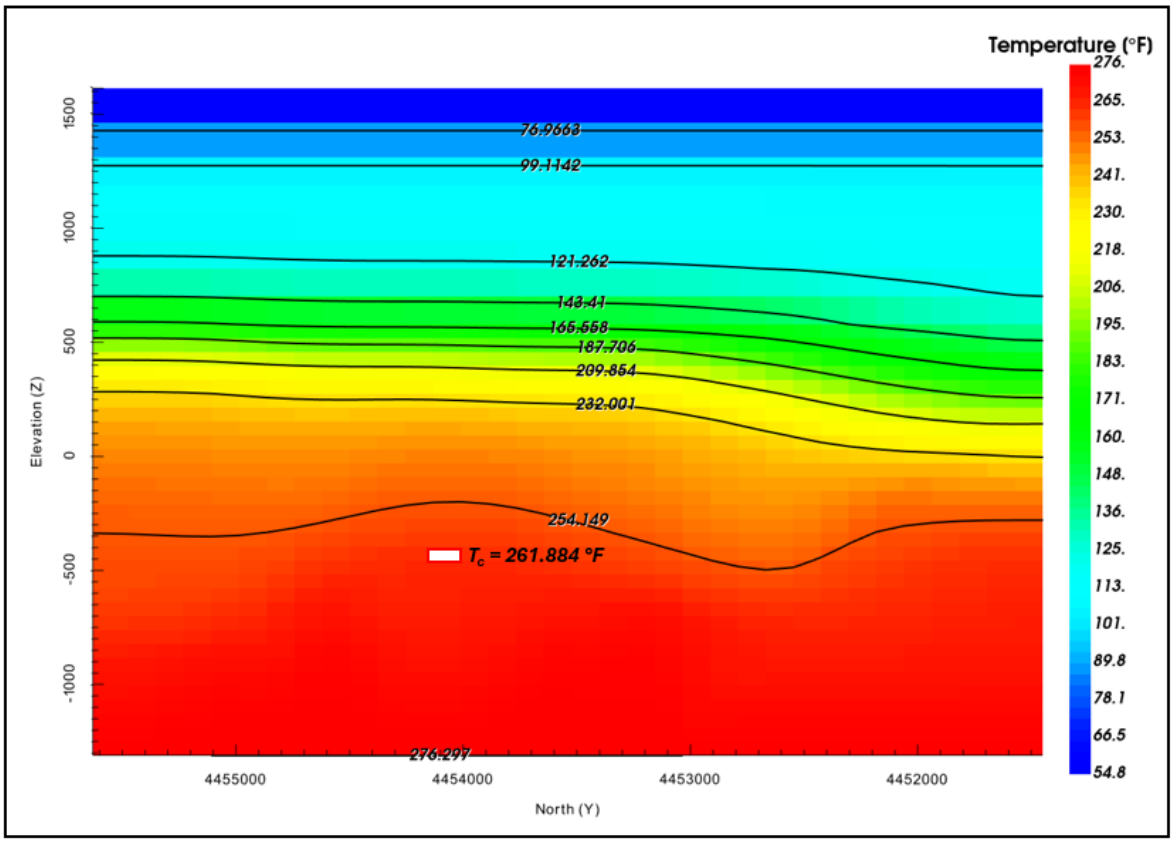

Figure 11: Simulation results of the thermal gradient for the natural-state reservoir simulation. T_c = 261.884°F for the cell containing the feedzone for Blackburn well no. 18, within 1°F of the temperature obtained from a recent well flowing test.

4. CONCLUSIONS

From the current phase 2 CGM, we have further supported the initial suggestion that the heat source is likely deep-seated. We have also estimated the thermophysical properties of the reservoir geological units, the locations of high-angle normal faults, the structure of fault blocks in the Devonian reservoir, and the trends in thickness of the overlying shale capping layer. The numerical simulation has provided an estimate of the thermal gradient through the subsurface, as well as shown the convective forces at work in the reservoir.

The following conclusions have been drawn from the completion of the Blackburn Field geological and numerical models:

- Utilizing non-geo-referenceable seismic interpretations can provide information about the general dip and strike/trend of the faults.
- Surface lineation and structures can be interpreted from DEM data to confirm the existence of major faults that extend from the surface to the subsurface.
- Hydrothermal fluid likely upwells at the intersection of faults in the CGM.
- The source of this structurally controlled geothermal reservoir is likely deep-seated.
- The temperature match for the field well flowing test was approximately 262°F.

Gaps in knowledge and data in this project arise from the lack of information about the reservoir (accurate temperature logs, unknown productivity indices of wellbores, etc.), and the inability to access original, time-interpreted 3D seismic data to ensure a more accurate conceptual and numerical representation of the geological volumes in the subsurface. Future versions of the CGM will include the import

of updated, time-interpreted 3D seismic data. The numerical model will include the updated CGM volumes, as well as information about sealing and non-sealing faults gleaned from tracer tests. The initial phase 1 and phase 2 CGMs, as well as the natural-state simulation, represent the subsurface to the best of our current knowledge and are likely to contain missing data points when compared to newer, updated data sources. The models developed over the course of the project may not be an entirely correct representation of the subsurface, but they are still useful for determining unknowns in the system, and possible paths forward regarding the exploration of the geothermal resource. The point of evolving a CGM, and by extension a numerical model of the reservoir, is to fill the gaps in knowledge about the geothermal resource as the exploration phase of the active geothermal project continues.

ACKNOWLEDGEMENTS

This work was authored by the National Renewable Energy Laboratory, operated by Alliance for Sustainable Energy, LLC, for the U.S. Department of Energy (DOE) under Contract No. DE-AC36-08GO28308. Funding provided by the U.S. Department of Energy Office of Energy Efficiency and Renewable Energy Geothermal Technologies Office. The views expressed herein do not necessarily represent the views of the DOE or the U.S. Government. The U.S. Government retains and the publisher, by accepting the article for publication, acknowledges that the U.S. Government retains a nonexclusive, paid-up, irrevocable, worldwide license to publish or reproduce the published form of this work, or allow others to do so, for U.S. Government purposes. Benjamin Burke, Russell Roundtree, Lia Sedillos, and Johanna Ostrum at Gradient Geothermal Inc. as well as Rod Prosceno and Gene Wadleigh at Grant Canyon Oil and Gas are gratefully acknowledged for the data that they have provided the authors and their insightful discussions.

REFERENCES

Ayling, B. F., & Hinz, N. H. (2020). Developing a conceptual model and power capacity estimates for a low-temperature geothermal prospect with two chemically and thermally distinct reservoir compartments, Hawthorne, Nevada, USA. Geothermics, 87, 101870. https://doi.org/10.1016/j.geothermics.2020.101870

Bahadori, A., & Holt, W. E. (2019). Geodynamic evolution of southwestern North America since the Late Eocene. Nature Communications, 10, 5213. https://doi.org/10.1038/s41467-019-12950-8

Blackwell, D. D., & Steele, J. L. (1989). Thermal Conductivity of Sedimentary Rocks: Measurement and Significance. In N. D. Naeser & T. H. McCulloh (Eds.), Thermal History of Sedimentary Basins (pp. 13–36). Springer New York. https://doi.org/10.1007/978-1-4612-3492-0_2

Carlisle, D., Nelson, C. A. (1990). "Geology of the Mineral Hill 15' Quadrangle, Eureka County, NBMG, Map 97 (GeoDataBase)." Nevada Bureau of Mines and Geology. Reno, Nevada. Digitized 2008, accessed August 2023.

Cavero, J., Orellana, N., Yemez, I., Singh, V., & Izaguirre, E. (2016). Importance of conceptual geological models in 3D reservoir modelling. First Break, 34. https://doi.org/10.3997/1365-2397.2016010

Davis, M. G., Chapman, D. S., Van Wagoner, T. M., & Armstrong, P. A. (2007). Thermal conductivity anisotropy of metasedimentary and igneous rocks. Journal of Geophysical Research: Solid Earth, 112(B5), 1–7. https://doi.org/10.1029/2006JB004755

Faulds, J. E., Hinz, N. H., Dering, G. M., & Siler, D. L. (2013). The Hybrid Model—The Most Accommodating Structural Setting for Geothermal Power Generation in the Great Basin, Western USA. Geothermal Resources Council Transactions 37:3-10.

Faulds, J. E., Coolbaugh, M. F., Vice, G. S., & Edwards, M. L. (2006). Characterizing structural controls of geothermal fields in the northwestern Great Basin: A progress report. 30, 69–76. Geothermal Resources Council Transactions.

Flanigan, T.E., 1994. Blackburn Field: Oil, above a low-angle detachment fault in Eureka County, Nevada. In Schalla, R.A., and Johnson, E.H. (eds.), Oil fields of the Great Basin, Nevada Petroleum Society, 380 pp.

Franz, P. & Clearwater, J. (Oct. 2023). Volsung User Manual Version 2.0.20231030. Flow State Solutions Ltd.

Hulen, J. B., Bereskin, R. S., & Bortz, L. C. (1990). High-Temperature Hydrothermal Origin for Fractured Carbonate Reservoirs in the Blackburn Oil Field, Nevada. The American Association of Petroleum Geologists, 74(2), 1262–1272.

Kutun, K., Gold, A., Beckers., K. (2023) Resource Characterization to Estimate Potential for Electricity Co-Production at Blackburn Oil Field, Nevada. Geothermal Resources Council Transactions.

Manger, G. E. (1963). Porosity and bulk density of sedimentary rocks (No. 1144-E). USGPO.

Nevada Bureau of Mines and Geology (NBMG). (2023). Oil and Gas Well Log Files (Search) [Database]. Nevada Bureau of Mines and Geology. https://nbmg.unr.edu/oil&gas/WellSearch.html

Oviedo, M. J., Blessent, D., López-Sánchez, J., & Raymond, J. (2023). Contribution to the characterization of the Nevado del Ruiz geothermal conceptual model based on rock properties dataset. Journal of South American Earth Sciences, 124, 104259. https://doi.org/10.1016/j.jsames.2023.104259

Pedersen, R. (2023, January 6). What Makes the Walker Lane so Special? [Article Page]. Convergent Mining. https://www.convergentmining.com/c-blog/grassroots-exploration-on-the-walker-lane

Porter, R. C., Fouch, M. J., & Schmerr, N. C. (2014). Dynamic lithosphere within the Great Basin. Geochemistry, Geophysics, Geosystems, 15(4), 1128–1146. https://doi.org/10.1002/2013GC005151

Pruess, K., Oldenburg, C. M., & Moridis, G. J. (1999). TOUGH2 User's Guide Version 2 (LBNL-43134). Lawrence Berkeley National Lab. (LBNL), Berkeley, CA (United States). https://doi.org/10.2172/751729

Pruess, K. (1992, May 1). Brief guide to the MINC-method for modeling flow and transport in fractured media (Report LBL--32195). Other Information: PBD: May 1992; Lawrence Berkeley Laboratory. https://doi.org/10.2172/10179280

Sass', J. H., Lachenbruch, A. H., Dudley, W. W., Priest', S. S., & Munroe, R. J. (1988). Temperature, thermal conductivity, and heat flow near Yucca Mountain, Nevada: Some tectonic and hydrologic implications (Open File 87–649; p. 26). UNITED STATES DEPARTMENT OF THE INTERIOR GEOLOGICAL SURVEY.

Schön, J.H. (Ed.) (2015) Physical Properties of Rocks: Fundamentals and Principles of Petrophysics. Developments in Petroleum Science, Vol. 65, Elsevier.

Schön, J.H. (2011). Physical Properties of Rocks: A Workbook (Handbook of Petroleum Exploration and Production). Elsevier.

Scott, C., & Chamberlain, A. K. (1988). Blackburn Field, Nevada: A Case History.

Snoke, A., Howard, K., Mcgrew, A. J., Burton, B., Barnes, C. G., Peters, M., & Wright, J. (1997). The grand tour of the Ruby-East Humboldt metamorphic core complex, northeastern Nevada: Part 1 - Introduction & road log. Brigham Young University Geology Studies, 42, 225–296.

Taverna, Nicole. (2019). Sedimentary Geothermal Feasibility in Eastern Nevada and Millard County, Utah Well Databases. United States. https://dx.doi.org/10.15121/1637461

University of Nevada, Reno. (2021). INGENIOUS Thermal Conductivity Measurement Source Categorization [data set]. Retrieved from https://dx.doi.org/10.15121/1874222.

USGS 10 m n41w117_20180206. (2018). DEM GeoTiff Map datafile. United States. Retrieved from https://apps.nationalmap.gov/lidar-explorer/#/

Waples, D. W., & Waples, J. S. (2004). A Review and Evaluation of Specific Heat Capacities of Rocks, Minerals, and Subsurface Fluids. Part 1: Minerals and Nonporous Rocks. Natural Resources Research, 13(2), 97–122. https://doi.org/10.1023/B:NARR.0000032647.41046.e7

Zhu, X., Gao, Z., Chen, T., Wang, W., Lu, C., & Zhang, Q. (2022). Study on the Thermophysical Properties and Influencing Factors of Regional Surface Shallow Rock and Soil in China. Frontiers in Earth Science, 10, 1–13. https://www.frontiersin.org/articles/10.3389/feart.2022.864548